Hybrid multiphoton and optoacoustic microscope

George J. Tserevelakis,† Dominik Soliman,† Murad Omar, and Vasilis Ntziachristos*

Institute for Biological and Medical Imaging, Technische Universität München and Helmholtz Zentrum München, Germany
**Corresponding author: v.ntziachristos@tum.de*

Received January 10, 2014; accepted February 8, 2014;
posted February 20, 2014 (Doc. ID 204576); published March 20, 2014

We present a hybrid microscope combining multiphoton microscopy incorporating second-harmonic generation contrast and optical-resolution optoacoustic (photoacoustic) microscopy. We study the relative performance of the two systems and investigate the complementarity of contrast by demonstrating the label-free imaging capabilities of the hybrid microscope on zebrafish larvae *ex vivo*, concurrently visualizing the fish musculature and melanocytes. This implementation can prove useful in multiparametric microscopy studies, enabling broader information to be collected from biological specimens. © 2014 Optical Society of America

OCIS codes: (110.0180) Microscopy; (110.5120) Photoacoustic imaging; (180.4315) Nonlinear microscopy.
http://dx.doi.org/10.1364/OL.39.001819

Over the past decades, a wide range of optical microscopy modalities utilizing different contrast mechanisms have been developed to reveal structure and function in biological specimens. Multiphoton microscopy represents a powerful modality at the forefront of microscopy approaches, offering optical diffraction-limited fluorescence imaging deep inside tissues and other scattering media. In addition to two-photon excitation, the use of second-harmonic generation (SHG) enables imaging of birefringence in orientated/organized biological structures such as collagen [1], myosin fibrils [2], microtubules [3], starch granules [4], etc. Therefore, SHG microscopy can provide valuable information not only regarding the molecular structure of many cellular components, but also their respective orientation in the three-dimensional space [5]. In this manner, SHG signal recording has the potential to offer intrinsic complementary contrast in a typical two-photon excitation fluorescence (TPEF) microscope by simply employing a very narrow bandpass interference filter transmitting light only at the half of the excitation wavelength. Additional contrast can be obtained in a stain-free manner from lipids [6], including lipid membranes and other cellular components by utilizing third-harmonic generation.

The combination of several modalities under a hybrid microscope has the potential to produce images of different contrast and provide complementary information that enhances the understanding of complex properties [7]. In this work, we combined two microscopy approaches, merging multiphoton microscopy and optoacoustic (photoacoustic) microscopy. Optoacoustic microscopy (OM) visualizes optical absorption by measuring laser-induced ultrasonic waves [8], a feature that is highly complementary to the contrast provided by two- or multiphoton microscopes. In the past, OM has been combined with fluorescence confocal microscopy [9]. However, compared to confocal microscopy, the previously undocumented development of hybrid multiphoton and optoacoustic microscopy (MPOM) offers better complementarity, because multiphoton microscopy is known to penetrate deeper into tissues than confocal microscopy, reaching depths similar to those achieved by OM [4]. Therefore, while a confocal fluorescence microscope images more superficially than an OM, the hybrid MPOM reported herein can provide images through similarly sized volumes, offering better potential for hybrid contrast coregistration. In addition, optoacoustic imaging has also been combined with optical coherence tomography [10] and other modalities [11–13].

The custom-built MPOM system, shown in Fig. 1, implemented a multiphoton microscope and an optical-resolution OM system. Therefore, the MPOM system presented herein was built to be highly compatible with multiphoton microscopy, both depth-wise and resolution-wise. Two-photon and SHG microscopy employed a femtosecond laser emitting at a central wavelength of 1043 nm (YBIX, Time-Bandwidth, Zurich, Switzerland; pulse width, 170 fs; output average power, 2.8 W; repetition rate, 84.4 MHz), enabling high peak powers for the

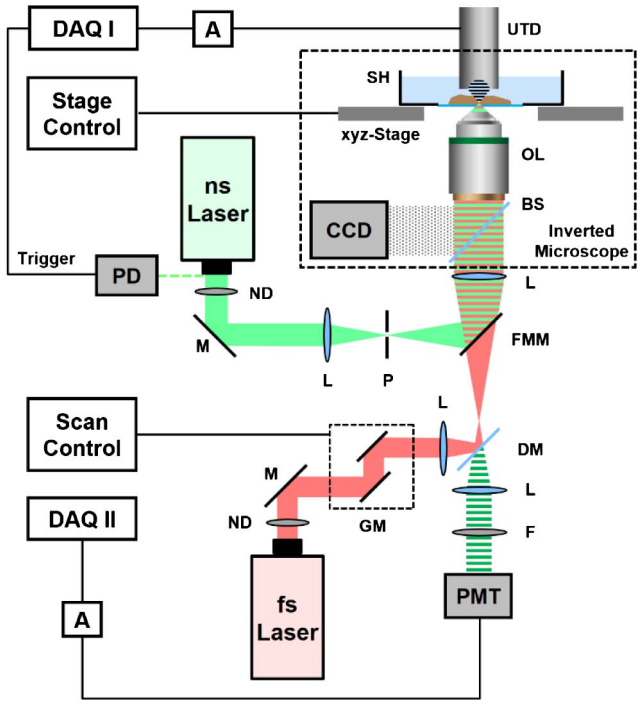

Fig. 1. Schematic of the integrated MPOM. ND, neutral density filter; L, lens; M, mirror; P, pinhole; FMM, flip-mount mirror; PD, photodiode; GM, galvanometric mirror set; DM, dichroic mirror; SH, sample holder; BS, beam splitter; F, optical bandpass filter; PMT, photomultiplier tube; OL, objective lens; UTD, ultrasound transducer; A, amplifier; DAQ, data acquisition system.

efficient excitation of nonlinear processes at relatively low pulse energies, however, so that a minimum sample disturbance was induced. The laser beam was initially attenuated, collimated, and finally guided onto a high-precision set of galvanometric mirrors (6215 H, Cambridge Technology, Bedford, Massachusetts, USA) to perform the raster scanning of the biological specimen in the xy plane. Subsequently, the beam was reflected by a suitable dichroic mirror (DMSP805R, Thorlabs, Newton, New Jersey, USA) and passed through a telescope system, expanding it in order to fill the back aperture of the employed high NA objective lens (Plan Apochromat 20X, Zeiss, Jena, Germany; air immersion, 0.8 NA), which tightly focused the excitation light into the specimen that was placed in a modified inverted optical microscope (AxioObserver.D1, Zeiss, Jena, Germany). Furthermore, the focal plane was selected via a high-resolution piezoelectric motorized translational z stage (MZS500-E, Thorlabs). The generated SHG signals were collected in the backward direction, following an inverse path through the objective lens and the visibly transparent dichroic mirror, to be detected using an appropriate bandpass interference filter (FB520-10, Thorlabs) via an ultrasensitive photomultiplier tube (H9305-03, Hamamatsu, Hamamatsu City, Japan) and finally to be recorded by a 16-bit data acquisition system (PCIe-6363, National Instruments, Austin, Texas, USA). The average power at the specimen was 65 mW, corresponding to a pulse energy of ~0.77 nJ. No photodamage effects have been noted when using these irradiation parameters. The observation of the specimen prior to the SHG imaging was achieved via a CCD camera (AxioCam ICc 1, Zeiss, Jena, Germany) and its respective positioning was performed using a motorized xy stage (MLS203-2, Thorlabs). The synchronization of the multiphoton setup devices was achieved through custom-designed programs written in LabVIEW, while the respective image processing was accomplished via MATLAB and ImageJ.

The optoacoustic subsystem employed tightly focused laser light obtained from a 515 nm DPSS laser (Flare HP PQ Green 2 k-500, Innolight GmbH, Hannover, Germany; energy per pulse, 570 μJ; pulse width, 1.8 ns) that irradiated the sample at 1.2 kHz. Focusing of the laser beam confined the region of acoustic wave generation to a small, optical diffraction-limited spot. Since the optical focus was much smaller than the acoustic focus of the ultrasound transducer (~20 μm), the lateral resolution was defined by the optical properties of the system, particularly the excitation wavelength and the NA of the employed objective lens [14]. After being attenuated, expanded, and spatially filtered by a 25 μm pinhole, the laser beam was coupled into the inverted microscope via a flip mount mirror, which enabled an easy switching between nonlinear and optoacoustic measurements. A 0.25 NA objective lens (PLN 10X, Olympus, Hamburg, Germany) was used to focus the light into the sample, which was placed on a glass slide. The pulse energy at the sample was ~6 nJ. The generated broadband acoustic waves were detected by a spherically focused 78 MHz ultrasonic transducer (SONAXIS, Besancon, France; F/D ≈ 1) that was positioned above the sample in a confocal and coaxial arrangement with respect to the optical focus. For good acoustic coupling, a few drops of deionized water were placed between the transducer and the sample, which was covered and fixed by means of a thin plastic foil. After amplification with a 63 dB amplifier (AU-1291, Miteq, New York, USA), the signals were recorded via a data acquisition card (Cobra Max CS23G8, Gage Applied, Lockport, USA; 8-bit resolution, 1.5 GS/s per channel). A fast photodiode (DET36A, Thorlabs) recorded scattered laser light and served as a trigger for the data acquisition. Since the optical illumination and transducer remained fixed during the experiments, the scanning was performed by moving the sample holder via the fast, high-precision xy stage that was mounted together with the piezoelectric z stage on top of the inverted microscope. The acquisition control, signal processing, and image generation were performed in MATLAB.

For characterizing the spatial resolution achieved by the multiphoton modality, we measured 100 nm diameter fluorescent beads (TetraSpeck Fluorescent Microspheres Size Kit, Invitrogen, Carlsbad, California, USA), which are much smaller than the full width at half-maximum (FWHM) of the diffraction-limited laser spot of ~665 nm, predicted by

$$R_{\text{lateral}} = 0.51\frac{\lambda}{\text{NA}}, \tag{1}$$

where λ stands for the excitation wavelength and NA for the numerical aperture of the objective lens. Figure 2 shows the profile plots of measured nanobeads in the (a) lateral and the (b) axial dimension. The profiles are fitted with a Gaussian curve ($R^2 = 0.999$ and 0.961, respectively). The insets in Fig. 2 depict images of one nanobead, imaged via the recording of TPEF signals in both (a) lateral and (b) axial views, corresponding to the measured point spread function (PSF) of the system, if we reasonably assume that the employed particles behave like fluorescing point sources. In the axial dimension, we observe a vertical elongation of the sphere, representative of the expected resolution achieved in the z direction. The FWHM of the curve for the PSF measured in the lateral view was found to be ~674 nm, a result which is comparable to the ideal diffraction-limited spot of the beam. Nevertheless, we have to note that due to the quadratic dependence of the process on the incident excitation intensity, one should expect a spot which

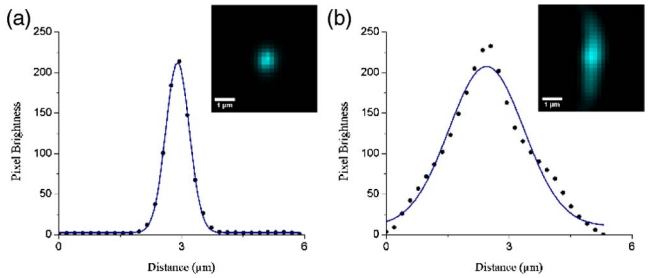

Fig. 2. Spatial resolution characterization of the multiphoton system. (a) Lateral profile of a 100 nm fluorescent nanobead with fitted Gaussian curve. (b) Axial profile of the nanobead. The insets show 2D images of the nanobead in the lateral and axial view.

would be smaller by a factor of $\sqrt{2}$ than the diffraction-limited one. However, in multiphoton microscopy, this intrinsic resolution improvement is usually not attained without the integration of specially designed adaptive optical systems, since the existing optical aberrations (spherical aberration, coma, etc.) can significantly reduce the focusing quality and lead to an extended, less confined focal volume of the excitation beam. As far as the axial resolution is concerned, the respective FWHM of the fitted Gaussian curve was estimated to be around 2.15 μm, nearly three times larger than its corresponding lateral extent.

In order to determine the lateral resolution of the OM system, we measured black polystyrene microspheres with 2.8 μm diameter (Polybead, Polysciences Inc., Warrington, Pennsylvania) embedded in pure agar. An image was acquired by scanning the sample in the xy plane in 0.2 μm steps. At each measurement position, the acoustic signals as a function of time were recorded and averaged five times. Subsequently, the signal envelopes were calculated, employing the Hilbert transform. The inset in Fig. 3 shows the maximum amplitude projection (MAP) along the z direction (corresponding to the time axis) of a single microsphere. The corresponding profile was fitted with a Gaussian function ($R^2 = 0.975$) and yielded a FWHM of 2.5 μm. Under the assumption that the optical illumination and the sphere's original MAP profile follow a Gaussian shape, the system's lateral resolution was finally estimated to be ~2.2 μm based on the expression

$$R_{\text{lateral,OM}} = \sqrt{d_{\text{exp}}^2 - d_{\text{sph}}^2}, \tag{2}$$

where d_{exp} represents the measured and d_{sph} the actual FWHM of the microsphere (assuming that the sphere diameter of 2.8 μm corresponds to $\pm 3\sigma$ of the Gaussian profile). This value is two times higher than the theoretical FWHM of the optical Airy disk of ~1.1 μm predicted by Eq. (1), which is probably due to optical aberrations and an imperfect laser beam quality. In contrast to the transverse resolution, the axial resolution in OM is governed by the properties of the employed ultrasound transducer and was determined to be ~7 μm in a previous experiment [15].

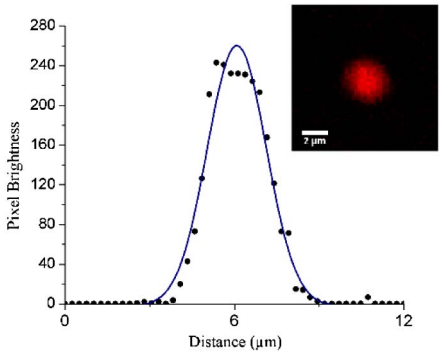

Fig. 3. Lateral resolution estimation of the OM. The graph shows the Gaussian fitted profile of a 2.8 μm microsphere. The inset illustrates the corresponding MAP of the sphere along the z axis.

To demonstrate the capabilities of the developed MPOM, we imaged an 11-day-old zebrafish larva (huC::GCamP5G) *ex vivo*. In general, fish offer a variety of biological structures of different contrast. Collagen and muscle fibers in the fish body are known to be efficient SHG emitters, since they possess strong birefringence properties that significantly enhance the nonlinear signal. In this study, we were particularly interested to identify whether the hybrid microscope could visualize and coregister the muscular system and melanocyte populations present in the larvae. For imaging, a brightfield image was captured through the microscope CCD camera as a reference and SHG and OM images were obtained from the same field of view. Figure 4(a) shows the merged two-component MPOM image. The red color represents a MAP of the optoacoustic signals collected, whereas the green color corresponds to the respective SHG signals. Optoacoustic responses are generated from the strongly absorbing regions populated by melanocytes at the two sides and the characteristic stripe along the center of the fish tail. The imaged structures appear to be in a very good agreement with the optically opaque regions in the recorded brightfield image shown in Fig. 4(b). Concerning the nonlinear modality, we initially removed the saturated pixels to improve the visibility of the obtained image. The SHG image reveals the fish muscles, which induce nonlinear responses. The spatial resolution of the setup is high enough to discriminate even several single fibrils constituting the muscular system of the fish. These highly orientated structures contribute to the modulation of the tissue's optical properties in order to render it as a birefringent medium, and are thus appropriate for efficient nonlinear signal generation.

The recorded multimodal image displays the label-free capabilities of the developed MPOM system, demonstrating the potential for label-free microscopy of biological specimens. The combination of second-harmonic contrast and optoacoustic contrast yielded herein the first insights, to our knowledge, into an interesting microscopy approach whereby cells and structures can be visualized even at the absence of labels. With the recorded ability of the optoacoustic method to provide spectral differentiation of different chromophores [16], a next step in this development would be the implementation

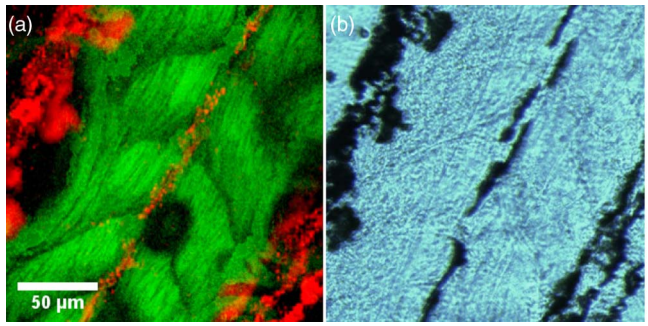

Fig. 4. Combined SHG and optoacoustic image of a zebrafish larva tail. (a) Hybrid image showing melanocytes (red) measured by the optoacoustic modality and muscle fibrils (green) recorded by the multiphoton system. (b) Brightfield image of the same tail region.

of multiwavelength illumination, which can further improve the differentiation of different labels and tissue structures with characteristic absorption spectra. In addition, an obvious next step is the utilization of this system with genetically modified biological specimens expressing fluorescent proteins or labeled with fluorescent moieties.

Multiphoton microscopy represents a powerful modality and it is ideally suited for integration with optical-resolution OM, both providing good resolution characteristics and similar depth penetration. Other hybrid implementations can be foreseen, however, most notably the combination of multiphoton microscopy or even MPOM with ultrasound-limited optoacoustic mesoscopy, enabling a system which can switch from 0.5–1 mm penetration and optical diffraction-limited resolution to 1–10 mm optoacoustic mesoscopy imaging with ultrasound diffraction-limited resolution.

Overall, the hybrid MPOM system presented herein offers the first insights, to our knowledge, into a hybrid label-free multiphoton and optical-resolution OM. It attains high potential for multiparameter microscopy, adding to the existing capacities of a multiphoton microscope the ability to image a variety of absorbing structures, ranging from visualizing hemoglobin and vasculature to resolving nanoparticles, including gold particles or labeled liposomes. Coupling of this system with third-harmonic generation could further lead to label-free imaging of an increasing number of tissue formations and cellular structures.

The authors would like to thank Prof. Gil Westmeyer and Dr. Antonella Lauri for providing them with the zebrafish larvae. VN acknowledges funding from an ERC Senior Investigator Award, a DFG Koseleck Award, and the TUM Excellence Initiative.

[†]These authors contributed equally to this work

References

1. R. Cicchi, N. Vogler, D. Kapsokalyvas, B. Dietzek, J. Popp, and F. S. Pavone, J. Biomed. Opt. **6**, 129 (2013).
2. P. J. Campagnola, A. C. Millard, M. Terasaki, P. E. Hoppe, C. J. Malone, and W. A. Mohler, Biophys. J. **82**, 493 (2002).
3. S. Psilodimitrakopoulos, V. Petegnief, G. Soria, I. Amat-Roldan, D. Artigas, A. Planas, and P. Loza-Alvarez, Opt. Express **17**, 14418 (2009).
4. N. Mazumder, J. Qiu, M. Foreman, C. Romero, P. Török, and F. Kao, Biomed. Opt. Express **4**, 538 (2013).
5. S. Psilodimitrakopoulos, V. Petegnief, N. De Vera, O. Hernandez, D. Artigas, A. M. Planas, and P. Loza-Alvarez, Biophys. J. **104**, 968 (2013).
6. G. J. Tserevelakis, E. V. Megalou, G. Filippidis, B. Petanidou, C. Fotakis, and N. Tavernarakis, PLoS ONE **9**, e84431 (2014).
7. C. Vinegoni, T. Ralston, W. Tan, W. Luo, D. L. Marks, and S. A. Boppart, Appl. Phys. Lett. **88**, 053901 (2006).
8. V. Ntziachristos, Nat. Methods **7**, 603 (2010).
9. Y. Wang, S. Hu, K. Maslov, Y. Zhang, Y. Xia, and L. V. Wang, Opt. Lett. **36**, 1029 (2011).
10. S. Jiao, Z. Xie, H. F. Zhang, and C. A. Puliafito, Opt. Lett. **34**, 2961 (2009).
11. H. F. Zhang, J. Wang, Q. Wei, T. Liu, S. Jiao, and C. A. Puliafito, Opt. Express **18**, 1278 (2010).
12. X. Zhang, H. F. Zhang, C. A. Puliafito, and S. Jiao, J. Biomed. Opt. **16**, 080504 (2011).
13. G. Langer, K. D. Bouchal, H. Grün, P. Burgholzer, and T. Berer, Opt. Express **21**, 22410 (2013).
14. R. Ma, S. Söntges, S. Shoham, V. Ntziachristos, and D. Razansky, Biomed. Opt. Express **3**, 1724 (2012).
15. M. Omar, J. Gateau, and V. Ntziachristos, Opt. Lett. **38**, 2472 (2013).
16. D. Razansky, M. Distel, C. Vinegoni, R. Ma, N. Perrimon, R. W. Köster, and V. Ntziachristos, Nat. Photonics **3**, 412 (2009).